Zitierweise: *Angew. Chem. Int. Ed.* **2021**, *60*, 1942–1950
Internationale Ausgabe: doi.org/10.1002/anie.202012851
Deutsche Ausgabe: doi.org/10.1002/ange.202012851

Dative Bonds

The Existence of a N→C Dative Bond in the C_{60}–Piperidine Complex

Maximilián Lamanec[+], Rabindranath Lo[+], Dana Nachtigallová, Aristides Bakandritsos, Elmira Mohammadi, Martin Dračínský, Radek Zbořil,* Pavel Hobza* and Weizhou Wang**

Abstract: *The complexes formed between carbon allotropes (C_{20}, C_{60} fullerenes, graphene, and single-wall carbon nanotubes) and piperidine have been investigated by means of computational quantum chemical and experimental IR and NMR techniques. Alongside hydrogen bonds, the C···N tetrel bond, and lone-pair···π interactions, the unexpected N→C dative/covalent bond has been detected solely in complexes of fullerenes with piperidine. Non-planarity and five-member rings of carbon allotropes represent the key structural prerequisites for the unique formation of a dative N→C bond. The results of thermodynamics calculations, molecular dynamics simulations, and NMR and FTIR spectroscopy explain the specific interactions between C_{60} and piperidine. The differences in behavior of individual carbon allotropes in terms of dative bonding formation brings a new insight into their controllable organic functionalization.*

Introduction

Buckmisterfullerene C_{60} (further named as fullerene (FL), Scheme 1), a ball-shaped compound, and its derivatives represent the class of carbon allotropes which received considerable attention due to their applications in bio-related[1–3] and material-chemistry fields.[4–6] Their unique cage structure, buckyball, greatly affects their aromaticity by distortion of the π-conjugation from planarity leading to a decrease of p-orbitals involved in the π-bonds and an increase of s-orbital contribution in sp^2 carbon atoms, respectively.[7] In particular, the energy of the lowest unoccupied orbitals (LUMO) decreases and, at the same time, the electron affinity of FLs increases. Determination of the electron affinity (EA) of C_{60} has been the subject of several experimental investigations[8] and has been approached by means of computational studies based on the DFT methods.[9] The EA value has been estimated as 2.684 eV.[8]

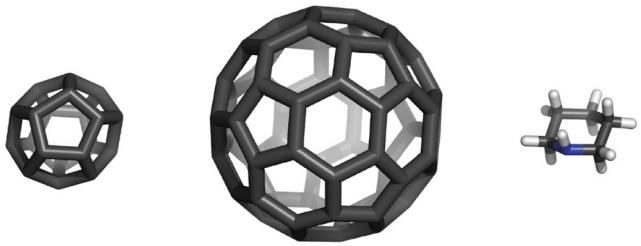

Scheme 1. Fullerenes C_{20} and C_{60} and pip ($C_5H_{11}N$).

The unusual electronic properties of FLs open the door to designing new materials via FL′s functionalization. However, what goes hand in hand with these excellent opportunities is a well-known problem of their solubility,[10] which shows very unusual behavior.[11] Frequently observed aggregation of FLs,[12] originating from the positive values of their EA, discussed above,[9] is one of the key drawbacks restricting the application potential of FL.

The behavior of C_{60} upon solvation, showing an increased solubility in aromatic compared to polar liquids, has been the subject of several experimental studies.[11,13–17] To explain these experimental observations, several theoretical and computational studies have been reported,[18–30] aiming to resolve the origin of solute-solvent interactions and to find the most relevant parameters to correlate the solvent properties and their efficiency to dissolve FLs.[18–22] Despite the strong basic character of piperidine (pip, $pK_a = 11.12$), which makes it an efficient electron donor, the explanation of the solubility based purely on the charge transfer is somewhat questionable, considering the low solubility of C_{60} in oxygen-containing solvents, alcohols, phenols and ketones.[20,22]

C_{60} is well known to form adducts[23–25] with primary and secondary amines, including pip. The reaction proceeds in the presence of oxygen under both, light and dark conditions, on a time-scale of days and with the yields of about 50%. The addition starts with an electron transfer C_{60} followed by

[*] M. Lamanec[+,++], R. Lo[+,++], D. Nachtigallová, M. Dračínský, R. Zbořil, P. Hobza
Institute of Organic Chemistry and Biochemistry
Czech Academy of Sciences
Flemingovo Náměstí 542/2, 16000 Prague (Czech Republic)
E-Mail: dana.nachtigallova@uochb.cas.cz
radek.zboril@upol.cz
pavel.hobza@uochb.cas.cz
M. Lamanec[+,++]
Department of Physical Chemistry, Palacký University Olomouc
tr. 17 listopadu 12, 771 46 Olomouc (Czech Republic)
R. Lo[+,++], D. Nachtigallová, A. Bakandritsos, E. Mohammadi
Regional Centre of Advanced Technologies and Materials
Faculty of Science, Palacký University
Šlechtitelů 27, 78371 Olomouc (Czech Republic)
W. Wang
College of Chemistry and Chemical Engineering, and Henan Key Laboratory of Function-Oriented Porous Materials
Luoyang Normal University, Luoyang 471934 (China)
E-Mail: wzw@lynu.edu.cn
R. Zbořil, P. Hobza
CATRIN, Šlechtitelů 27, 78371 Olomouc (Czech Republic)
[+] These authors contributed equally to this work.
[++] co-first authors.
Supporting information and the ORCID identification number(s) for the author(s) of this article can be found under: https://doi.org/10.1002/anie.202012851.

radical recombination and the zwitterion formation, which stabilizes either by proton transfer to C_{60}, forming C–H bond, or by oxidation and consequent deprotonation and radical recombination.

We have examined the character of the interactions in the complexes of pip with C_{20} (1:1), C_{60} (1:*n*) and its fragment $C_{30}H_{20}$ (1:1), all containing five-member rings, as well as in the graphene, modelled with circumcoronene, and graphene nanotubes, modelled with $C_{54}H_{18}$ and $C_{228}H_{38}$, respectively, although solely containing six-member rings. The calculations were performed by the dispersion-corrected-DFT method, employing the PBE0-D3[26] functional, whose reliability was verified on the basis of the comparison with the results obtained from pip···pip (pip_2) and C_{20}···pip complexes by the method of high-accuracy CCSD(T). The interactions are described in terms of both interaction and binding free energies at 298 K. To provide a more realistic picture of the solvation, molecular dynamics simulations were performed on C_{60} in pip droplet containing up to 21 molecules of the solvent at 298 K. The experimental results obtained by means of FTIR and (H,C)-NMR spectroscopies fully support the predicted character of the C_{60}···pip interaction.

Our results demonstrate the formation of the dative bond between the electron donor (secondary amine pip) and the electron acceptor (FL), qualitatively different from the addition of secondary amines to FLs under light and in the presence of oxygen, which occurs through oxidation of the previously formed ion pair between FLs and secondary amines.[25,27,28] A dative bond represents a type of covalent bond, hence the name covalent/dative bond, in which one fragment donates two electrons to the bond, unlike the electron sharing bond formed from the interactions of one unpaired electron of both fragments.[29,30]

We clearly proved that the changes in the aromaticity of non-planar carbon allotropes, previously explained by a smaller overlap of p-orbitals, differ for systems that contain five-member rings with respect to those constructed purely from six-member rings.[31]

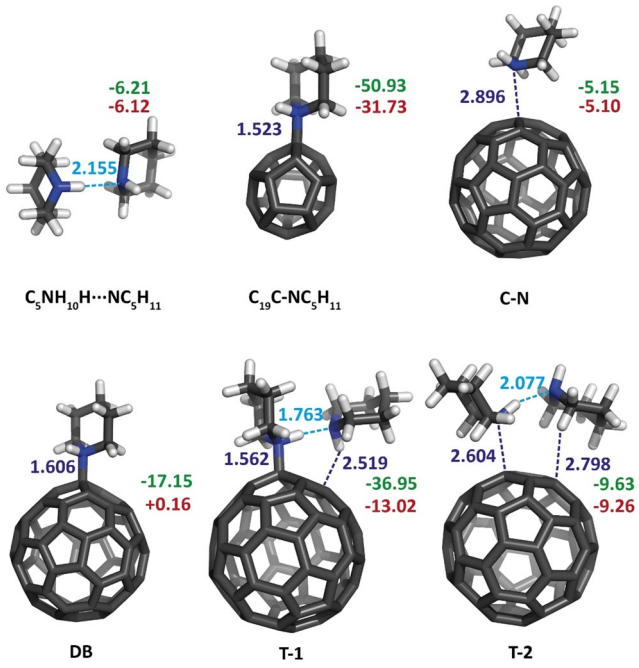

Figure 1. PBE0-D3/def2-TZVPP optimized geometry of pip_2, C_{20} with pip, C_{60} with pip, and C_{60} and pip_2 with selected bond lengths between fullerene and pip in Å (dark blue), hydrogen bond lengths between pips (light blue) in Å, and ΔE^{INTR}(green), and ΔE (red) in kcal mol^{-1}.

Tabelle 1: Intrinsic interaction energies (ΔE^{INTR}, in kcal mol^{-1}) of pip_2 and C_{20}···pip complexes.

Method	CCSD(T)[a]		MP2				DFT[b]
N	D	T	D	T	Q	5	
pip_2	−3.8	−4.7	−3.8	−5.0	−5.4	−5.6	−6.2 (−6.1)[c]
C_{20}···pip	−30.2	−43.2	−29.3	−37.0	−40.1	−41.3	−50.9 (−31.7)[c]

[a] cc-pVnZ basis set. [b] def2-TZVPP. [c] Total interaction energy (ΔE) is given in parentheses.

Results and Discussion

Interaction Energies

The character of interactions between the solvent molecules is investigated using pip dimer, the H-bonded complex with the N–H···N H-bond length of 2.16 Å (in Figure 1). The size of the system also allows employing the benchmarking DFT method to model the C_{60} solvation. The interaction energies of pip_2 dimer calculated using PBE0-D3/def2-TZVPP, MP2 and CCSD(T) methods are given in Table 1. The negligible difference between ΔE and ΔE^{INTR} indicates only marginal structure changes upon complexations. The DFT method provides slightly larger stabilization energies, and its comparison with the benchmark CCSD(T) calculations makes room for discussion, also based on the MP2 calculations. When the triple-zeta basis sets are used, the DFT overestimates the interaction energies by 1.5 and 1.2 kcal mol^{-1}, in comparison with CCSD(T) and MP2 methods, respectively. The more flexible cc-pV5Z basis set gives the energy difference of 0.6 kcal mol^{-1}, thus the DFT interaction energies are overestimated by about 10%. As the DFT method is known to be less basis-set-dependent, compared to the discussed wave-function methods, the error in DFT-calculated binding energies is not expected to significantly exceed the observed 10%, with respect to the CCSD(T) results extrapolated to the complete basis set (CBS) limit. The fair agreement between the MP2 and CCSD(T) stabilization energies which makes the former method suitable for benchmarking of C_{60} systems stabilization energies where the CCSD(T) calculations are not computationally feasible.

The optimized structure and properties of C_{20}···pip complex are displayed in Figure 1 and Table 1. The N–C distance in the complex is 1.523 Å, only slightly larger than the typical values of covalent C–N bonds (the optimized C–N bonds in pip are 1.453 Å). Notably, the similar type of interaction as described in the current paper has been already reported for the complex between C_{20} and N_2H_2.[32] Importantly, ΔE^{INTR}

calculated at the PBE0-D3/def2-TZVPP level is 50.9 kcal mol^{-1}, almost identical to ΔE^{INTR} value of 49.9 kcal mol^{-1} obtained for the N→B dative bond in ammonia borane (H_3NBH_3) addressed as the prototype dative complex. In conclusion, the short intermolecular distance and large stabilization energy indicate the formation of a new chemical entity with the dative bond between N (pip) and C (C_{20}). Several types of dative bonds have been reported previously.[29,33–41]

The difference between the ΔE and ΔE^{INTR} values of about 19 kcal mol^{-1} shows a significant structure deformation upon complexation. Assuming changes in the MP2 interaction energies with the increasing basis set, the PBE0-D3/def2-TZVPP approach is expected to provide results of the binding energies with an error of about 10%, compared to extrapolated reference CCSD(T) levels. Our results obtained with PBE0-D3 functional are in good agreement with those calculated for $C_{20}\cdots N_2H_2$, that is, complex with two C–N bonds, employing M06-2X functional and 6-311G(d,p) basis set, which gives the interaction energy of −57.8 kcal mol^{-1} and the bond length of 1.472 Å.[32]

The optimization of C_{60}···pip provides a more complex picture with a large variety of local minima, including non-covalent complexes and the complex with the N→C dative bond. Their structures, characterized by C···N intermolecular distances and intrinsic and total interaction energies obtained by the PBE0-D3/def2-TZVPP approach are given in Figure 1 (Supporting Information, Figure S1) and Table 2. In the former complex type pip is attached to C_{60} via non-covalent NH···C and CH···C hydrogen bonds (NH-C and CH-C structures, respectively), the C···N tetrel bond[42] (C–N structure) with bond lengths of 2.6–2.9 Å and the lone-pair (N)···π noncovalent interaction to five-(LP-R5) or six-membered (LP-R6) structures with bond lengths of about 3.1 Å. Their ΔE^{INTR} and ΔE values are within 1.1 kcal mol^{-1} (Table 2).

Figure 1 displays two optimized complexes, labeled C-N and DB, with similar mutual orientations of C_{60} and pip, leading to different orientations of the N (pip) lone pair, with respect to the C_{60} buckyball structure, significant differences in intermolecular C···N distances (cf. 2.896 Å and 1.606 Å for C-N and DB, respectively) and ΔE^{INTR} values (see Table 2) of −5.2 and −17.2 kcal mol^{-1}, respectively. By comparison, the interaction energies for the stacked configurations of the complex C_{60}···benzene are in the range of −5.49 to −4.13 kcal mol^{-1}.[19]

The values of the interaction energies in DB deserve a detailed discussion, based also on the comparison with non-covalent complexes and C_{20}···pip. In particular, the negative value of the intrinsic interaction energy ($\Delta E^{INTR} = -17.2$ kcal mol^{-1}) is compensated by an almost identical value of the deformation energy, leading to slightly repulsive interactions of +0.2 kcal mol^{-1}. The large deformation energy (cf Table S3) is explained by a distortion of C_{60} in DB, compared to the regular buckyball structure of the other non-covalent C_{60}···pip complexes (see Figure 1), with negligible deformation energies not larger than 0.05 kcal mol^{-1} (Table 2).

The existence of the N→C dative bond in the C_{60}-pip system was also verified using MP2 (see Table 2). The interaction energy in DB with the N→C dative bond is slightly larger at the DFT level, in agreement with the previous observation on the C_{20}···pip. The MP2 method, however, predicts ΔE^{INTR} in non-covalent complexes to increase by about 2 kcal mol^{-1}, which is consistent with the well-known overestimation of the dispersion energy at the MP2 level.

Although the N→C dative bond was predicted in C_{60}···pip complex, the large deformation energy casts doubt on its existence. However, the above-discussed stability is based on the gas-phase calculations, and only one pip molecule is considered. The description of C_{60}···pip interactions in pip solvent requires calculations of models with more solvent molecules and will proceed in two directions: analyses of the C_{60} complex with pip_2 and with pip droplet containing up to 21 pip molecules.

The complexes of C_{60} with pip_2 investigated in this study include binding via a dative bond (T-1, Figure 1) and non-covalent N···C bonds (T-2, Figure 1). Both, total and intrinsic interaction energies (see also Table 3) are calculated with respect to pip_2, in which pip molecules are labeled as *inner* and *outer* pip.

In the case of the T-1 complex, pip subunits bound to C_{60} via the N→C dative bond (*inner* pip), with the bond length of 1.562 Å (cf. 1.606 Å in DB), and the NH···C hydrogen bond (*outer* pip), with the bond length of 2.519 Å Figure 1 (cf. 2.557 Å in NH-C; Supporting Information, Figure S1). It should be noted that the H-bond between the pip subunits in $C_{60}\cdots pip_2$ significantly shortens (by 0.39 Å), compared to the H-bond in pip_2. The intrinsic interaction energy is analyzed in terms of partial energies of the *inner* and *outer* pip subunits in Table 3. Binding of the former is increased by about 3 kcal mol^{-1} and decreased by 1 kcal mol^{-1} in the case of the *outer* pip, respectively. The difference between their sum and the value of the total intrinsic interaction energy (13 kcal mol^{-1}, cf. the ΣE_{part} and ΔE^{INTR} values in Table 3) demonstrates the significant cooperative effect on the binding of the two pip subunits. Despite the large value of the deformation energy of 24 kcal mol^{-1}, the whole complex is stable with the

Tabelle 2: The intrinsic interaction energies (ΔE^{INTR}, in kcal mol^{-1}) and total interaction energies (ΔE, in kcal mol^{-1}) of C_{60}···pip complexes.

	C-N	LP-R6	LP-R5	NH-C	CH-C	DB
ΔE^{INTR} (MP2)	−7.1	−6.9	−7.2	−6.3	−6.8	−14.0
ΔE^{INTR} (DFT)	−5.2	−5.0	−5.0	−4.5	−4.1	−17.2
ΔE (DFT)	−5.1	−5.0	−5.0	−4.5	−4.1	+0.2

Tabelle 3: Total and partial intrinsic interaction energies (ΔE^{INTR}, kcal mol^{-1}) for $C_{60}\cdots pip_2$ complex.

System	E_{part}		ΣE_{part}	ΔE^{INTR}
	ΔE^{INTR} (*inner* pip)[a]	ΔE^{INTR} (*outer* pip)[b]		
T-1	−20.36	−3.67	−24.03	−36.95 (−13.02)[c]
T-2	−4.48	−3.89	−8.76	−9.63 (−9.26)[c]

[a] calculated as the difference between ΔE^{INTR} energy of $C_{60}\cdots pip_2$ and ΔE^{INTR} of C_{60}···*outer* pip. [b] Calculated as the difference between ΔE^{INTR} energy of $C_{60}\cdots pip_2$ and ΔE^{INTR} of C_{60}···*inner* pip. [c] The total interaction energies (ΔE in kcal mol^{-1}) are given in parentheses.

total interaction energy of −13 kcal mol^{-1}, unlike the slightly unstable DB 1:1 complex. The larger stability of the T-1 can be explained by a charge transfer cascade in the sequence *outer* pip → *inner* pip → C_{60}, which results in a larger charge separation, compared to DB. Consequently, the electron density at N involved in the N→C dative bond increases and the bond strengthens. The increased charge transfer is reflected in the changes in the NBO populations (Supporting Information, Table S4) of the σ*(N-H) antibonding orbital, calculated as 0.017 in an isolated pip molecule, 0.030 in H-bonded pip dimer, 0.026 in DB and 0.101 in T-1, respectively. The difference between the populations of the two former corresponds with the formation of the N(lone pair)···σ*(N-H) H-bonded pip_2 complex ($\Delta E^{INTR} = -6.20$ kcal mol^{-1}, Table 1). The large population of the corresponding σ*(N-H) in T-1 evidences a significant charge transfer to C_{60} accompanying the formation of the strong the N→C dative bond ($\Delta E^{INTR} = -20.36$ kcal mol^{-1}, Table 3).

In T-2, the *inner* pip interacts with C_{60} via the C···N tetrel bond (relevant to C-N structure) and the *outer* pip bounds via the C-H···C (C_{60}) H-bond. The N-H···N H-bond within the pip_2 subunit shortens by about 0.08 Å, compared to the pip_2 dimer. The strength of the C_{60}···*inner* pip interactions is comparable (within the range of 0.6 kcal mol^{-1}) to the corresponding C···N interaction in the C-N complex (Figure 1), although the bond distance is significantly, by 0.29 Å, smaller in C-N. Unlike for T-1, comparable values of ΣE_{part} and ΔE^{INTR} indicate almost additive contributions of *inner* and *outer* pip subsystems to the overall stabilities of T-2; the cooperative effects do not account for more than 10% of the total ΔE^{INTR}. Further, the deformation energy is significantly smaller.

The above-discussed results on T-structures show important differences in the potential energy surface (PES) characters of C_{60}···pip_2 and C_{60}···pip. In particular, the slightly unstable DB complex stabilizes upon the extension with an additional H-bonded pip in T-1, which, in contrast to DB, becomes more stable than the non-covalent T-2, and corresponds to the global minimum on the C_{60}-pip_2 PES. These changes indicate enhanced electron-acceptor properties of C_{60} in the presence of other pip molecules, along with a preferential formation of dative bond when C_{60} dissolves in pip. The hydrogen bond enhanced strength of the dative bond can be thus regarded as a subclass of noncovalent cooperativity.[43,44] The existence of several minima of C_{60} complexes, such as those found in C_{60}···pip on PES along single-coordinate (C···N), has been reported previously on other complexes of C_{60}.[45]

The calculations on the carbon allotropes with six-membered rings only do not confirm the existence of dative/covalent bond. In this case, only the non-covalent complexes are formed (see discussion on FTIR spectra, Supporting Information).

C_{60}···pip_{21}. The solubility of C_{60} in pip (modelled with 21 pip molecules) was investigated using the PBE0-D3/6-31G* approach. The performance of the less flexible basis set was verified by comparing the interaction energies in smaller complexes with C_{20} and C_{60} (Supporting Information, Table S5). Figure 2a displays the optimized structure of C_{60}···pip_{21} and the intrinsic interaction energy showing one pip interacting via the N→C dative bond and the remaining pip molecules via non-covalent interactions. The intrinsic interaction energies of C_{60}···pip_{20} with one molecule of pip_2 (cf T-1 complex) being removed, interacting either non-covalently (Figure 2c) or via the dative bond (Figure 2b), are shown to illustrate their mutual effects on the complex stability. The sum of the intrinsic interaction energies of the former complex (Figure 2c) and dative C_{60}···pip complex (Figure 2d) is −116.3 kcal mol^{-1}, which is by 26 kcal mol^{-1} less than the interaction energy calculated for the full C_{60}···pip_{21} complex (−142.4 kcal mol^{-1}), demonstrating a significant synergy effect of the non-covalent interaction and the N→C dative bond. In particular, the formation of the dative bond increases the electron density of C_{60}, leading to stronger N−H···C and C−H···C hydrogen bonds. Similarly, the sum of the intrinsic interaction energy in Figure 2b (−123.4 kcal mol^{-1}) and energies of two missing H-bonds (ca. 12 kcal mol^{-1}) is lower than ΔE^{INTR} of the C_{60}···pip_{21} (Figure 2a) by about 7 kcal mol^{-1}. This difference can be related to the above-discussed enhancement of the interaction strength of the dative bond in the hydrogen bonded pip_2.

More details on the dissolution mechanism were obtained with calculations displayed in Figure 3. Different initial structures with one, two and three pip molecules attached with N→C dative bond to C_{60} and the H-bond to the neighboring pip molecule, respectively, were optimized using the PBE/6-31G* approach (for justification of the PBE-D3 approach see the results of thermodynamics terms in the Supporting Information, Table S5). The calculations show that the most stable arrangement is with two N→C dative bonds, followed by the complex with one and three N→C dative bonds, less stable by 11.2 and 22.1 kcal mol^{-1}, respectively. It should be noted that the last structure resulted from

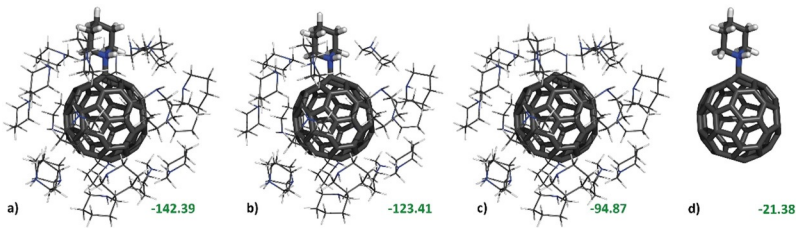

Figure 2. PBE0-D3/6-31G(d) interaction energies of the complexes C_{60}···$(C_5H_{11}N)_{21}$ (a), C_{60}···$(C_5H_{11}N)_{20}$ (b) with dative bond, C_{60}···$(C_5H_{11}N)_{20}$ (c) without dative bond and C_{60}···$C_5H_{11}N$ (d). The geometries of C_{60}···$(C_5H_{11}N)_{20}$ and C_{60}···$C_5H_{11}N$ are extracted from the PBE0-D3/6-31G(d) optimized geometries of C_{60}···$(C_5H_{11}N)_{21}$.

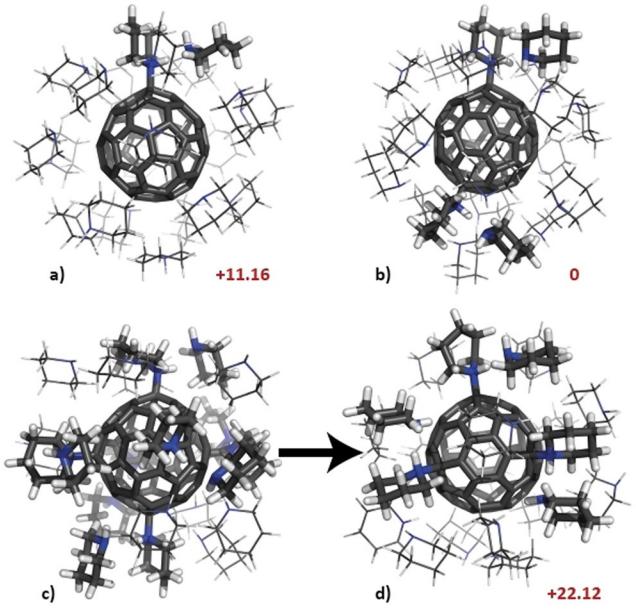

Figure 3. PBE-D3/6-31G* optimized geometry of $C_{60}\cdots pip_{21}$ complex. Structure a) contains one dative bond, structure b) two and structure d) three dative bonds. Optimization of starting structure c) having six dative bonds led to structure d) with three dative bonds. Numbers in red correspond to relative energies in kcal mol^{-1}.

the optimization of the complex with six dative bonds (see Figures 3c,d), which corresponds to the previously stated expectation of the limited ability of C_{60} to form dative bonds with pip.

The free energy calculations (see the Supporting Information for details) support the thermodynamic stability of the of $C_{60}\cdots pip_2$ also at temperature 298 K.

The dative bond was confirmed also using MD simulations of $C_{60}\cdots(pip)_{21}$ performed at 300 K for 0.1 ns. Results are shown in the Supporting Information, section 2.

FTIR Spectra

The FTIR spectra of C_{60} and its mixture with pip before and after the evaporation of some excess amount of unbound pip molecules (labeled C_{60}-P1 and C_{60}-P2, respectively) are shown in Figure 4. The spectrum of the pip alone shows the collective band at 1000–1200 cm^{-1} due to the C–N bond and skeletal -C-N-C stretches[46,47] (Figure 4a), which is in good agreement with the calculated value of 1242 cm^{-1} (intensity 17 km mol^{-1}). The bands of the C-N stretch of pip also dominate the spectrum obtained after the mixing and grinding of pip with C_{60} (Figure 4a, spectrum C_{60}-P1). After evaporation of excess pip, new bands at 872 cm^{-1} and 988 cm^{-1} appear in the spectrum (Figure 4a, spectrum C_{60}-P2), assigned in calculations (Supporting Information, Table S2c and Figure S4) to symmetric (866 cm^{-1}, 383 km mol^{-1}) and asymmetric (994 cm^{-1}, 46 km mol^{-1}) stretches of dative N→C bond in C_{60}-pip_2 complex.

The spectra in the frequency region higher than 3000 cm^{-1} reflect the changes of N-H stretching vibrations of pip. The calculated N-H stretching frequency of the pip (Supporting Information, Table S2a) is 3514 cm^{-1} with a negligible intensity of 1 km mol^{-1}. Upon the pip_2 and pip_3 formation, these bonds are either involved in hydrogen bonding (NH-bond) or remain non-bonded (NH-free). The corresponding band of the former is red-shifted to 3401 cm^{-1}, with intensity of 275 km mol^{-1}, in the case of a single H-bond pip_2 and to 3306 and 3340 cm^{-1} (intensities of 434 and 461 km mol^{-1}) owing to a combined more curved later structure bands of the two hydrogen bonds in pip_3 (Supporting Information, Table S2). Both, the red-shift and the increased intensity manifest the well-known effect of the hydrogen bond formation. The frequencies and intensities of the NH-free bonds do not change. Based on these calculations, the band at 3280 cm^{-1} visible in the spectra of pip and C_{60}-P1 (Figure 4b) can be assigned to the N-H stretch of the NH-bonds in the pip solvent. In the C_{60} -P2 spectrum, the intensity of the band at 3280 cm^{-1} decreases and, at the same time, a new band at 3444 cm^{-1} appears (Figure 4b). The calculations predict a strongly shifted (by 300 cm^{-1}) and high-intensity peak (2705 cm^{-1}, 1534 km mol^{-1}) in the $C_{60}\cdots pip_2$ complex for the NH-bond, which is, however, hidden within the C–H vibra-

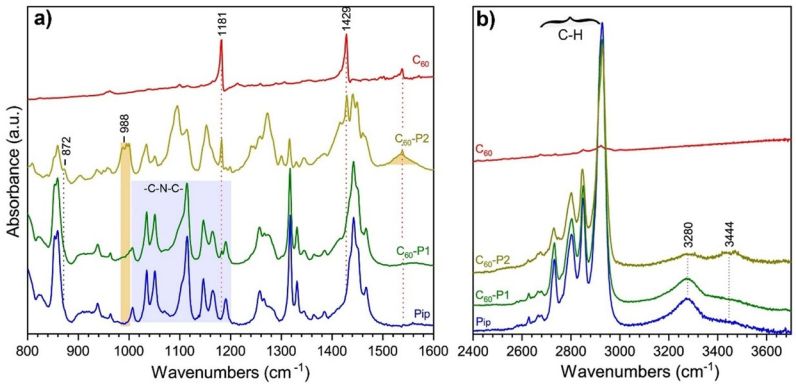

Figure 4. FTIR spectra of C_{60} and its complex with pip (Pip) before evaporation (C_{60}-P1) and after evaporation of some excess amount of unbound pip (C_{60}-P2) at two spectral windows for the observation of (a) the C-N stretching and N-H bending vibrations, and (b) the N-H stretching vibrations.

tional stretching bands (see Figure 4b). Inspection of the calculated vibrational frequencies and intensities of the NH-free bonds in pip, C_{60}···pip and C_{60}···pip_2 reveal both a red-shift and an intensity increase. Based on this and the geometry parameters obtained from the T-1 optimization (the distance between H (*outer pip*) and C(C_{60}) is 2.5 Å, Figure 1), the discussed band at 3444 cm^{-1} in C_{60}-P2 can be linked to the N-H stretch of the outer pip interacting with C_{60} via van der Waals interactions. It should be noted that the C-H vibrations of the pip observed in the frequency region of 2700–3000 cm^{-1} are retained without changes (Figure 4b).

The changes observed in the spectral region of 1500–1600 cm^{-1}, relevant to the N-H bending modes, provide additional information about the character of C_{60} interaction with pip. The characterization of the peaks due to the NH-free bending in pip_2 and pip_3 is similar to that of pip monomer, that is, the frequency of ≈1520 cm^{-1} and a low intensity of about 7 km mol^{-1} (Supporting Information, Table S2b). The formation of hydrogen bonds within the pip cluster (pip_2, pip_3) results in the blue-shift of the bands by about 70 cm^{-1}, keeping a negligible intensity (Supporting Information, Table S2). In the case of the interaction with C_{60}, the blue-shift is smaller (ca. 40 cm^{-1}) but the intensity is increased to 43 km mol^{-1} (Supporting Information, Table S2). These calculations provide the bases for the interpretations of the band at 1540 cm^{-1}, observed solely in the C_{60}-P2 spectrum, to the bending mode of the NH-bond of the *inner* pip in which the N atom interacts with the electron acceptor (from formation of a dative bond or non-covalent interactions (see below)). Therefore, this new band excludes the possibility of the complexation via the addition of secondary amines to FL, accompanied by oxidation,[25,27,28] since the corresponding hydrogen atom is released upon this reaction.

The FTIR spectra of the mixture of pip with graphene (Gr) and single wall nanotubes (NT) are illustrated in the Supporting Information, Figures S5 and S6, respectively, in the same spectral regions as discussed for the complex with C_{60}. The bands of the starting graphene material at 1272 and 1575 cm^{-1} (Supporting Information, Figure S5a, Gr) are attributed to two different vibrational modes of conjugated aromatic rings in the graphene sheet with defects. Concerning the spectral signs linked to the complex formation between C_{60} and pip: 1) the band at about 3500 cm^{-1} (assigned to 3444 cm^{-1} in C_{60}-P2, see above for its interpretation), and 2) the band at about 1550 cm^{-1} (assigned to 1540 cm^{-1} in C_{60}-P2, see above for its interpretation) become prominent in the spectra of the mixture of pip with Gr or NT. This observation is confirmed by computational modelling of the interactions of pip_2 with circumcoronene, representing Gr surface, and a NT fragment (Supporting Information, Figure S6). In both cases, the optimization results in a structural arrangement similar to that of T-2.

Importantly, the bands at 872 and 998 cm^{-1}, due to the stretching modes of the N→C dative bond, are missing in both spectra, demonstrating the inefficiency of these allotropes to form a dative bond with pip.

NMR Spectroscopy

Figure 5 displays the ^{1}H-NMR and ^{13}C-NMR spectra of pure C_{60}, pure pip, and their mixtures in deuterated 1,2-dichlorobenzene. In the aliphatic (pip) region of the proton NMR spectrum of the C_{60}-pip mixture, the broad signal at about 3.4 ppm and narrow signal at about 1.9 ppm correspond to hydrogens in alpha- (H2) and beta-(H3) positions with respect to nitrogen, respectively. The signal due to hydrogens in gamma- position (H4) in the complex is overlapped by the very intense peak of free pip. Its chemical shift can be obtained from two-dimensional proton-carbon correlation experiment (Supporting Information, Figures S8–S14). The lack of the signal due to the NH proton can result either from its overlap with other signals and/or its severe broadening. The chemical shifts of the C–H hydrogens are higher in complexes than in free pip, with the differences 0.53 ppm (H2), 0.29 ppm (H3) and 0.07 ppm (H4), respectively, indicating their smaller shielding in the complex and thus a decrease of electron density upon complexation. The largest

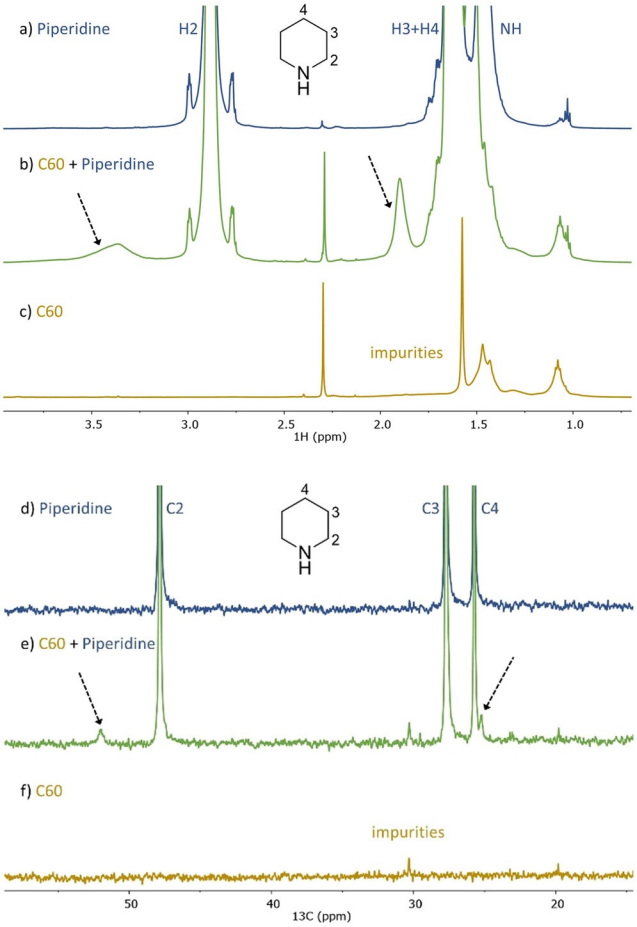

Figure 5. Part of ^{1}H NMR (top) and ^{13}C (bottom) spectra of 1,2-dichlorobenzene-d_4 (550 µL) solutions of a,d) pip (20 µL), b,e) mixture of C_{60} (14.7 mg) and pip (20 µL) and c,f) C_{60} (14.7 mg). The black dashed arrows highlight the signals of the C_{60}-pip complex. Full spectra (including the aromatic region) and spectra with variable amounts of pip are shown in the Supporting Information.

difference in chemical shift observed for H2 indicates a direct involvement of pip N-atom in the complex formation.

Similar to H-NMR spectra, two new signals appear in the aliphatic part of C-NMR spectra of pip and C_{60} mixture, demonstrating the complex formation. Comparison of the differences of chemical shifts of pip C-atoms shows the most pronounced shift for C2 (4.1 ppm), in agreement with corresponding differences observed in H-NMR spectra. The signal corresponding to C3 in the complex is overlapped by that of free pip. Furthermore, new signals appear also in the C_{60} region at 140–150 ppm (Supporting Information, Figure S10). Importantly, no signals are observed in the region of 70–80 ppm, characteristic for addition (that is, covalent bond formation) of secondary amines to C_{60}.[25]

The spectral characterization, that is, the shape and intensity of signals, provides further characterization of the complex behavior. The broader signals due to H2 in the C_{60}-pip complex as compared to free pip can be explained by multiple complex formation (multiple complex structures) and their dynamic behavior, that is, $C_{60}\cdots(pip)_n \leftrightarrow C_{60}\cdots(pip)_{n-1}$ + pip equilibria. The multiple signals observed in the spectra obtained with variable pip concentration (Supporting Information, Figure S10) confirm the presence of multiple complex structures, that is, complexes with one or more pip molecules. The dynamic behavior of the C_{60}-pip complex can be deduced from variable temperature NMR experiments (Supporting Information, Figure S14). Narrowing of the broad signal and intensity decrease observed at elevated temperatures indicate that the signals correspond to metastable species which satisfy the above equilibrium between the complex and its components.

The intensity of the signals of the C_{60}-pip complex are significantly lower than those of the free components. Considering C_{60} and pip concentrations, the integration of the signals in proton NMR spectra can be used to determine the complex concentration and to estimate the complexation free energy. The estimated value of ΔG value at 25 °C is -0.1 kcal mol^{-1}, which is in excellent agreement with the calculated value for $C_{60}\cdots pip_2$ (Supporting Information, Table S5).

Preconditions for the Formation of a N→C Dative Bond: Structural Aspects

Unusual reactivity of carbon allotropes is related to their different structural and electronic properties. Our results concerning the formation of the N→C dative bond between pip and C_{20} or C_{60}, constructed either exclusively from the five-member rings or from both five- and six-membered rings, confirm this explanation. The observed character of the binding of pip to carbon nanotubes, which contain solely six-member rings, raises the question whether the out-of-planarity deviation is the only prerequisite to alter the aromaticity. More detailed analyses of the curvature effect were made by calculations performed on carbon allotropes with six-member rings modelling nanotubes with different diameters, 7 and 15 Å (Supporting Information, Figure S7), which corresponded to those of C_{60} and experimentally used NT, respectively. The data displayed in the Supporting Information show an absence of dative complexes with pip and confirm our experimental and computational observations of the structural requirement, that is, the presence of five-member rings to form such complexes.

To provide an explanation for the different behavior of allotropes with and without five-member rings, the calculations were performed for the $C_{30}H_{20}\cdots pip_2$ complex, in which the $C_{30}H_{20}$ fragment represents the half of the C_{60} buckyball (Figure 6a). The $C_{30}H_{20}$ is the largest C_{60}-fragment, which can possibly vary the degree of cage curvature in its equilibrium structure. Both, full and partial optimizations of the complex were performed. The full optimization of the complex resulted in a non-covalent complex (Figure 6b, C_{30}(opt)) characterized by a small ΔE^{INTR} value of -7.56 kcal mol^{-1} (Table 4) and relatively large C-N distance of 3.28 Å. During the optimization procedure, the $C_{30}H_{20}$ fragment slightly opens and the curvature of the bowl becomes smaller. In the partial optimization, the $C_{30}H_{20}$ structure was cut from T-1 and kept frozen (Figure 6c). The resulting ΔE^{INTR} of -18.78 kcal mol^{-1} (Table 4) and C–N bond distances of 1.58 Å indicate formation of the complex (labeled as $C_{30}(C_{60})$) with one N→C dative bond. The EA values of isolated C_{30}(opt) and $C_{30}(C_{60})$ fragments (Table 4) significantly differ with the more positive EA value for the more curved later structure. These values correlate well with aromaticity parameters derived from the harmonic oscillator model of aromaticity (HOMA).[48] Using this approximation, the HOMA index fits into the interval HOMA = 0 for the Kekule structure of benzene and HOMA = 1 for aromatic benzene. The values of 0.89 and 0.93 for the 5- and 6-member ring of C_{30}(opt) show its more aromatic character compared to $C_{30}(C_{60})$ with the values of 0.69 and 0.85, respectively. Importantly, the drop of the aromaticity index is significantly larger in the case of the five-member ring (by 0.2) between C_{30}(opt) and $C_{30}(C_{60})$ compared to the lowering by 0.08 for the six-member ring. This result indicates more pronounced structure effects on the aromaticity in the former and provides

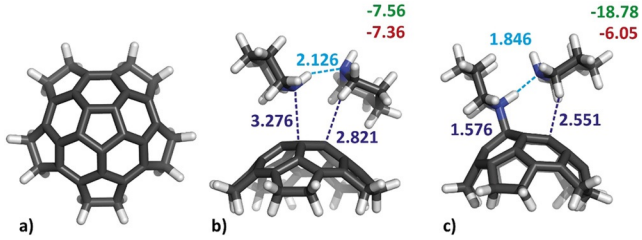

Figure 6. PBE0-D3/def2-TZVPP optimized geometries of $C_{30}H_{20}$ with selected hydrogen bond lengths between pips (light blue) in Å, and ΔE^{INTR}(green) and ΔE (red) in kcal mol^{-1}.

Tabelle 4: The interaction energies (ΔE^{INTR}, kcal mol^{-1}), electron affinity (EA, in eV) and HOMA values of $C_{30}H_{20}\cdots pip_2$ complexes.

Structures	ΔE^{INTR}	EA	HOMA	
			5-membered ring	6-membered ring
C_{30}(opt)	−7.56	+0.21	0.887	0.926
$C_{30}(C_{60})$	−18.78	+0.45	0.693	0.846

explanation for surprisingly different reactivity of non-planar carbon allotropes, carbon nanotubes, constructed from six-member rings only.

Conclusion

The results of computational modelling and experimental IR and NMR studies of the complexes of a secondary amine, pip, and various carbon allotropes have been performed to provide insight into the unusual behavior of FLs with respect to other carbon allotropes. It has been shown that the positive electron affinity resulting from non-planarity of carbon framework is responsible for the formation of the covalent/dative bond between pip and FL, in particular C_{60}. Analyses of the aromaticity of carbon allotropes revealed that not only their non-planarity but also the structural motives present in the carbon framework determine the character of the electron affinity, along with their ability to form the covalent/dative bond. This observation is demonstrated on a different bonding character of pip to C_{20} and C_{60} FLs, containing five-member rings, compared to that of pip to single wall carbon nanotubes that were constructed solely from six-member rings. The present observations provide information about the reactivity-structure relations of carbon allotropes potentially useful for their simple and selective covalent functionalization applicable to a broad portfolio of nanotechnologies.

Acknowledgements

M.L. acknowledges the Palacký University Internal Grant Association (IGA PrF_2020_022). W.W. gratefully acknowledges the National Science Foundation of China (21773104) for funding. The support of the Czech Science Foundation, the projects 19-27454X (R.L., D.N., A.B., R.Z., and P.H.) and 18–11851S (M.D.) is also acknowledged. E.M. thanks the ERDF-ESF „Nano 4 Future“ (No. CZ.02.1.01/0.0/0.0/16 019/0000754). We thank Michal Hocek for inspiring and helpful discussion and Tomáš Steklý for technical assistance in sample preparation and FTIR data collection.

Conflict of interest

The authors declare no conflict of interest.

Stichwörter: covalent functionalization · fullerenes · hydrogen bonds · N→C dative bonds · piperidine

[1] E. De Gianni, E. Turrini, A. Milelli, F. Maffei, M. Carini, A. Minarini, V. Tumiatti, T. Da Ros, M. Prato, C. Fimognari, *Toxins* **2015**, *7*, 535 – 552.
[2] C. M. Sayes, A. M. Gobin, K. D. Ausman, J. Mendez, J. L. West, V. L. Colvin, *Biomaterials* **2005**, *26*, 7587 – 7595.
[3] N. Gharbi, M. Pressac, M. Hadchouel, H. Szwarc, S. R. Wilson, F. Moussa, *Nano Lett.* **2005**, *5*, 2578 – 2585.
[4] K. A. Mazzio, C. K. Luscombe, *Chem. Soc. Rev.* **2015**, *44*, 78 – 90.
[5] W. Cao, J. Xue, *Energy Environ. Sci.* **2014**, *7*, 2123 – 2144.
[6] S. Günes, H. Neugebauer, N. S. Sariciftci, *Chem. Rev.* **2007**, *107*, 1324 – 1338.
[7] M. Saito, H. Shinokubo, H. Sakurai, *Mater. Chem. Front.* **2018**, *2*, 635 – 661.
[8] D. L. Huang, P. D. Dau, H. T. Liu, L. S. Wang, *J. Chem. Phys.* **2014**, *140*, 224315.
[9] J. Luo, L. M. Peng, Z. Q. Xue, J. L. Wu, *J. Chem. Phys.* **2004**, *120*, 7998 – 8001.
[10] N. O. Mchedlov-Petrossyan, *Theor. Exp. Chem.* **2020**, *55*, 361 – 391.
[11] R. S. Ruoff, R. Malhotra, D. L. Huestis, D. S. Tse, D. C. Lorents, *Nature* **1993**, *362*, 140 – 141.
[12] N. O. McHedlov-Petrossyan, *J. Mol. Liq.* **2011**, *161*, 1 – 12.
[13] N. O. McHedlov-Petrossyan, *Chem. Rev.* **2013**, *113*, 5149 – 5193.
[14] R. S. Ruoff, D. S. Tse, R. Malhotra, D. C. Lorents, *J. Phys. Chem.* **1993**, *97*, 3379 – 3383.
[15] M. V. Korobov, A. L. Mirakyan, N. V. Avramenko, G. Olofsson, A. L. Smith, R. S. Ruoff, *J. Phys. Chem. B* **1999**, *103*, 1339 – 1346.
[16] K. N. Semenov, N. A. Charykov, V. A. Keskinov, A. K. Piartman, A. A. Blokhin, A. A. Kopyrin, *J. Chem. Eng. Data* **2010**, *55*, 13 – 36.
[17] F. Cataldo, *Fullerenes Nanotubes Carbon Nanostruct.* **2009**, *17*, 79 – 84.
[18] J. S. Peerless, G. H. Bowers, A. L. Kwansa, Y. G. Yingling, *J. Phys. Chem. B* **2015**, *119*, 15344 – 15352.
[19] M. M. Li, Y. B. Wang, Y. Zhang, W. Wang, *J. Phys. Chem. A* **2016**, *120*, 5766 – 5772.
[20] M. T. Beck, G. Mándi, *Fuller. Sci. Technol.* **1997**, *5*, 291 – 310.
[21] S. Talukdar, P. Pradhan, A. Banerji, *Fuller. Sci. Technol.* **1997**, *5*, 547 – 557.
[22] D. Mahdaoui, M. Abderrabba, C. Hirata, T. Wakahara, K. Miyazawa, *J. Solution Chem.* **2016**, *45*, 1158 – 1170.
[23] G. Schick, K. D. Kampe, A. Hirsch, *J. Chem. Soc. Chem. Commun.* **1995**, 2023 – 2024.
[24] A. Hirsch, Q. Li, F. Wudl, *Angew. Chem. Int. Ed. Engl.* **1991**, *30*, 1309 – 1310; *Angew. Chem.* **1991**, *103*, 1339 – 1341.
[25] Y. Li, L. Gan, *J. Org. Chem.* **2014**, *79*, 8912 – 8916.
[26] C. Adamo, V. Barone, *J. Chem. Phys.* **1999**, *110*, 6158 – 6170.
[27] K. N. Semenov, N. A. Charykov, I. V. Vorotyntsev, *Russ. J. Phys. Chem. A* **2015**, *89*, 1206 – 1210.
[28] H. Isobe, N. Tomita, E. Nakamura, *Org. Lett.* **2000**, *2*, 3663 – 3665.
[29] L. Zhao, M. Hermann, N. Holzmann, G. Frenking, *Coord. Chem. Rev.* **2017**, *344*, 163 – 204.
[30] T. Clark, J. S. Murray, P. Politzer, *Phys. Chem. Chem. Phys.* **2018**, *20*, 30076 – 30082.
[31] E. F. Sheka, *J. Struct. Chem.* **2006**, *47*, 593 – 599.
[32] R. Ghiasi, M. Z. Fashami, A. H. Hakimioun, *J. Theor. Comput. Chem.* **2014**, *13*, 1450023.
[33] A. Haaland, *Angew. Chem. Int. Ed. Engl.* **1989**, *28*, 992 – 1007; *Angew. Chem.* **1989**, *101*, 1017 – 1032.
[34] C. J. Cramer, W. L. Gladfelter, *Inorg. Chem.* **1997**, *36*, 5358 – 5362.
[35] C. Lepetit, V. Maraval, Y. Canac, R. Chauvin, *Coord. Chem. Rev.* **2016**, *308*, 59 – 75.
[36] H. Braunschweig, R. D. Dewhurst, L. Pentecost, K. Radacki, A. Vargas, Q. Ye, *Angew. Chem. Int. Ed.* **2016**, *55*, 436 – 440; *Angew. Chem.* **2016**, *128*, 447 – 451.
[37] U. B. Demirci, *Int. J. Hydrogen Energy* **2017**, *42*, 9978 – 10013.
[38] M. Fu, S. Pan, L. Zhao, G. Frenking, *J. Phys. Chem. A* **2020**, *124*, 1087 – 1092.
[39] M. L. Green, P. Jean, M. C. Heaven, *J. Phys. Chem. Lett.* **2018**, *9*, 1999 – 2002.
[40] C. F. Pupim, A. J. L. Catão, A. López-Castillo, *J. Mol. Model.* **2018**, *24*, 283.
[41] A. Nandi, S. Kozuch, *Chem. Eur. J.* **2020**, *26*, 759 – 772.

[42] A. Bauzá, T. J. Mooibroek, A. Frontera, *Angew. Chem. Int. Ed.* **2013**, *52*, 12317 – 12321; *Angew. Chem.* **2013**, *125*, 12543 – 12547.
[43] A. M. S. Riel, R. K. Rowe, E. N. Ho, A. C. C. Carlsson, A. K. Rappé, O. B. Berryman, P. S. Ho, *Acc. Chem. Res.* **2019**, *52*, 2870 – 2880.
[44] G. A. Jeffrey, *Crystallogr. Rev.* **2003**, *9*, 135 – 176.
[45] T. E. Shubina, D. I. Sharapa, C. Schubert, D. Zahn, M. Halik, P. A. Keller, S. G. Pyne, S. Jennepalli, D. M. Guldi, T. Clark, *J. Am. Chem. Soc.* **2014**, *136*, 10890 – 10893.
[46] P. Larkin, *Infrared and Raman Spectroscopy: Principles and Spectral Interpretation*, **2011**, Elsevier, Waltham, MA, USA.
[47] Y. S. Mary, H. T. Varghese, C. Y. Panicker, M. Girisha, B. K. Sagar, H. S. Yathirajan, A. A. Al-Saadi, C. Van Alsenoy, *Spectrochim. Acta Part A* **2015**, *150*, 543 – 556.
[48] E. D. Raczyńska, M. Hallman, K. Kolczyńska, T. M. Stepniewski, *Symmetry* **2010**, *2*, 1485 – 1509.

Manuskript erhalten: 22. September 2020
Akzeptierte Fassung online: 6. Oktober 2020
Endgültige Fassung online: 24. November 2020